Bioactive Materials 4 (2019) 322–333

Contents lists available at ScienceDirect

Bioactive Materials

journal homepage: http://www.keaipublishing.com/biomat

In-vitro bioactivity evaluation and physical properties of an epoxy-based dental sealer reinforced with synthesized fluorine-substituted hydroxyapatite, hydroxyapatite and bioactive glass nanofillers

Bahaa Abdulrazzaq Jerri Al-Bakhsh[a,b,1], Farhad Shafiei[c,1], Atieh Hashemian[c], Kiana Shekofteh[c], Behnam Bolhari[d], Marjan Behroozibakhsh[c,*]

[a] Department of Dental Biomaterials, School of Dentistry, Tehran University of Medical Sciences, Tehran, Iran
[b] Department of Conservative Dentistry, Dental School of University of Basra, Basra, Iraq
[c] Department of Dental Biomaterials, School of Dentistry/Research Center for Science and Technology in Medicine, Tehran University of Medical Sciences, Tehran, Iran
[d] Department of Endodontic, School of Dentistry, Tehran University of Medical Sciences, Tehran, Iran

ARTICLE INFO

Keywords:
Bioactivity
Bioactive glass
Epoxy-based dental sealer
Hydroxyapatite
Fluorine-substituted hydroxyapatite

ABSTRACT

The purpose of this study was to evaluate the physical properties and bioactivity potential of epoxy-based dental sealers modified with synthesized bioactive glass (BAG), hydroxyapatite (HA) and fluorine substituted hydroxyapatite (FHA) nanoparticles.

The synthesized powders were incorporated at 10% and 20% into the epoxy-based dental sealer. The setting time, flow and solubility and microhardness of the modified and unmodified samples were examined. The bioactivity was evaluated using FESEM-EDX and elemental mapping, ATR-FTIR and XRD.

The flow value of all of the experimental groups except the FHA modified samples, was greater than 20 mm. Concerning solubility, no specimens exhibited more than 1% weight loss. The solubility value of the FHA groups was statistically significant lower than other groups ($p \leq 0.001$). The mean hardness values of all of the modified samples were significantly higher than the unmodified group ($p \leq 0.001$).

Regarding bioactivity, *in vitro* study revealed that after 3 days immersion in SBF a compact and continuous calcium phosphate layer formed on the surface of epoxy sealers containing BAG and HA nanoparticles.

Based on these results, the addition of BAG and HA nanoparticles did not adversely alter the physical properties of epoxy sealers. Additionally, they improved the *in vitro* bioactivity of the epoxy sealer.

1. Introduction

Endodontic sealers have been classified according to their main components to zinc oxide, eugenol-based, calcium hydroxide, glass ionomers, epoxy resin-based; methacrylate resin-based; silicone-based; and bioceramic sealers [1]. Epoxy-based dental sealers were first introduced by Schroeder [2], and now widely used because of their good adhesion to dentin [3], tight apical seal, low solubility, and long-term dimensional stability [4].

Root canal sealers are in direct contact with the periapical tissue, and thus ideally, they should bess composed of a bioactive material [5]. A bioactive dental material should induce the deposition of carbonated apatite crystals—the main mineral phase of bone and dental hard tissues. The bioactivity of a root canal sealing material is related to its chemical composition and depends on the interaction between the bioactive material and its surrounding environment [6]. Mineral trioxide aggregate (MTA) and new tricalcium silicate (TCS) based cements such as Biodentine™ are some examples of bioactive dental sealers [7].

Different attempts have done to incorporate bioactive fillers including bioactive glasses (BAG) [8–10], nanostructured hydroxyapatite (nHA) [6], niobium, and zirconium oxide radiopacifiers [5], into root canal filling materials. These have been added to improve their sealing ability especially in the apical regions of root canal system. Alhashimi et al. [8] evaluated the bioactivity and the cytocompatibility of an experimental BAG-reinforced polyethylene root-canal filling composite and described that this may be a proper material for a root canal system

Peer review under responsibility of KeAi Communications Co., Ltd.
* Corresponding author. Department of Dental Biomaterials, School of Dentistry, Tehran University of Medical Sciences (TUMS), Ghods Street, Keshavarz Blv, Tehran, Iran.
E-mail address: behroozibakhsh@tums.ac.ir (M. Behroozibakhsh).
[1] Equal contribution.

https://doi.org/10.1016/j.bioactmat.2019.10.004
Received 27 August 2019; Received in revised form 13 October 2019; Accepted 15 October 2019
Available online 28 October 2019

due to its biocompatibility, bioactivity, low melting temperature, and easy removal [8], Collares et al. [6]added nanostructured HA (nHA) fillers to methacrylate-based root canal sealers and concluded that the addition of nHA up to 40% to root canal sealers did not alter the film thickness or radiopacity [6]. Heid et al. [9], incorporated nanometric and micrometric BAG particles into an epoxy resin sealer and resulted quicker calcium phosphate precipitation for nanometric BAG particles compared to the micrometric ones [9].

Bioactive glass is a known bioactive material first developed by Hench et al. [11]. BAG particles are mainly composed of SiO_2, CaO, Na_2O, and P_2O_5 in different ratios and are extensively used in dentistry due to their ability to induce HA formation when subjected to physiological fluids [11,12]. The potential for releasing remineralizing ions and HA precipitation makes BAG a potential source of a remineralizing agent in dental composites [12].

Hydroxyapatite (HA; $Ca_5(PO_4)_3OH$) has also been extensively used in the field of dentistry due to its remarkable biocompatibility, bioactivity, and similarity to the mineral phase of teeth and bone [13,14]. Several researchers have developed dental composites using HA fillers to improve their mechanical [15], antibacterial [16,17] and bioactivity properties [18].

Biological apatites usually contain a wide variety of other substitutions—one of the most common is the substitution of a fluoride ion for a hydroxyl ion [19,20]. Partial substitution of OH by F forms fluoride-substituted hydroxyapatite (FHA, $Ca_5(PO_4)_3(OH)_{1-x}F_x$) [21]. This substitution can reduce the volume of the unit cell. The density and the chemical stability of the lattice then increases due to the electrostatic bonding between the fluoride and the adjacent ions [22].

Moreno et al. reported that partially fluorine-substituted hydroxyapatite is more stable than either pure hydroxyapatite or fluoroapatite. They obtained the lowest Ksp for the solid solution phase of $Ca_5(PO4)_3(OH)_{0.43}F_{0.57}$ [23]. The high lattice stability of partially fluoridated hydroxyapatite can be explained by the formation of OH–F bonds and disordering in the orientation of OH^- ions by F^- [23,24].

This study assessed the effect of incorporation of sub-micron sized BAG, HA, and FHA particles on the physical properties and bioactivity of epoxy-based endodontic sealers. The null hypotheses were as follows: (1) The addition of sub-micron sized BAG, HA, and FHA would not affect the physical properties (setting time, flow, solubility, and hardness) of the epoxy resin sealer; (2) The addition of sub-micron BAG, HA, and FHA particles would not improve the bioactivity of the epoxy-based dental sealer.

2. Materials and methods

2.1. Synthesis of sub-micron sized HA and FHA particles

The HA and FHA powders were synthesized and characterized as previously described [25]. Briefly 0.015 M diammonium hydrogen phosphate solution (12 g; 99%, Merck Company) was slowly added to 0.09 M calcium nitrate solution with vigorous stirring. The pH of the solution was brought to 11 with concentrated 1 M sodium hydroxide solution (Merck Company). The resulting precipitate was aged for 24 h while being stirred at room temperature and then centrifuged and washed three times with deionised water. The resulting powder then was dried. To prepare the FHA powder, 10 g of prepared HA powder was suspended in 500 mL of 0.02 M sodium fluoride (98.5%, Merck company) solution. The pH of the solution was adjusted to 7 overnight. Then, the pH was decreased to 4 by slowly adding 1 M nitric acid (68%, Merck Company). After 30 min, the pH was changed to 7 via 1 M sodium hydroxide. This pH cycle was repeated three times. The solution was then centrifuged and washed with deionised water three times. The resulting wet powders were dried. Both HA and FHA powders were calcined at 600 °C for 1 h at the rate of 5 °C/min in air.

2.2. Synthesis of BAG nano-particles (nBAG)

The nBAG were synthesized using the sol-gel method. Briefly, 5.8 mol TEOS (tetraethylorthosilicate) was added to 1 M nitric acid solution and mixed for 60 min to fulfil the hydrolysis process. Here, 5.8 mol TEP (triethylphosphate), 0.17 mol calcium nitrate tetra-hydrate, and 0.32 mol sodium nitrate ($NaNO_3$) were added and allowed to react for 60 min. The transparent solution was stored for 5 days at room temperature and, after the storage period, gel formation occurred. The resulting gel was aged for 24 h at 70 °C, dried for 24 h at 120 °C, and calcined for 4 h at 700 °C to stabilize the structure and remove the remaining nitrates [26]. All synthesized powders were ball-milled at 1200 rpm for 10 min.

2.3. Characterization of synthesized powders

The synthesized HA, FHA, and BG powders were characterized using a combination of X-ray diffraction (XRD), Fourier transform infrared spectroscopy (FTIR), and field emission scanning electron microscopy micrographs (FESEM).

2.3.1. X-ray diffraction analysis

Phase analysis of the prepared powders was carried out using XRD (INEL EQUINOX 2000 diffractometer) with Cu-Ka radiation of 1.540598 Å working at 40 mA, 40 kV, and a scan speed of 0.02 s^{-1} in the 2θ range of 10–80.

2.3.2. Scanning electron microscopy

The powders were coated with a thin layer of gold (Au) by sputtering for conductivity; the microstructure of the powders were observed with FESEM (FEI Nova NanoSEM 450, Netherlands).

2.3.3. Fourier transform infrared spectroscopy

The synthesized powders were also investigated using FTIR (Nicolet iS50, USA) with the KBr pellet method upon addition of 0.2 g anhydrous KBR to 2 mg of synthesized powders. Data were collected at a resolution of 4 cm^{-1} and wavenumbers ranging between 400 and 4000 cm^{-1}.

2.4. Sample preparation of modified and unmodified epoxy-based dental sealer

To evaluate the effect of synthesized powders on physical properties (setting time, flow, hardness, and solubility) and bioactivity of epoxy-based dental sealers the specimens for each test study were assigned to seven groups according to the kind and percentage of added nanoparticle powders: (1) unmodified (control), (2) BAG/10%, (3) BAG/20%, (4) HA/10%, (5) HA/20%, (6) FHA/10%, and (7) FHA/20%. For the preparation of the un-modified groups, the powder and liquid of a silver-free commercially available AH26 epoxy resin sealer (Dentsply Maillefer –USA) were mixed according to the manufacturer's instructions. The composition of the powder and liquid included bismuth oxide (70%) with hexamethylene tetramine (25%) and bisphenol A-diglycidylether (BADGE), respectively [27].

To prepare the modified groups, the powder of conventional epoxy sealer was blended with 10 wt% and 20 wt% of each synthesized powder as follows. The synthesized powders and the AH26 sealer powder (Dentsply Maillefer USA) were weighed with an analytical balance (Sartorius, Goettingen, Germany) and divided into equal parts. Each part of the synthesized powders was mixed manually with commercially epoxy sealer (powder) for 3 min and then mixed with an amalgamator (Ultramat 2, SDI, Australia) to ensure adequate particle distribution.

The modified and unmodified powders were mixed with commercially epoxy resin liquid on a glass slab using a metal spatula with a powder-to-liquid (P/L) ratio of 2/1 as recommended by the

manufacturer. All prepared samples were placed into an incubator at 37 °C and 100% humidity to ensure complete polymerization.

2.5. Physical properties

The physical properties of the modified and unmodified samples including, setting time, flow, and solubility were evaluated according to the ISO 6876 specifications [28]. The microhardness value of the samples was also measured using a Vickers diamond indenter.

2.5.1. Setting time

To evaluate setting time, the mixed sealers were stored at 37 ± 1 °C and 95% humidity for 9 h. When the shortest setting time stated by the manufacturer (10 h) approached, a Gilmore-type needle indenter with a mass of 100 ± 0.5 g and a flat end 2.0 ± 0.1 mm in diameter was lowered vertically onto the surface of each specimen (10 mm width and 2 mm high) until the indentations were no longer visible. Five determinations were performed for each group.

2.5.2. Flow

A volume of 0.5 mL of each experimental sealer was put on the centre of a glass plate (40 mm, 40 mm, 5 mm) using a graduated insulin syringe. At 180 ± 5 s after the mixing began, the second plate (mass of 20 ± 2 g and load of 100 g) was placed onto the top surface of the prepared specimens. Seven minutes later, the applied load was removed, and the diameters of the compressed sealer discs were measured using a digital calliper with a resolution of 0.01 mm. The average of the major and minor diameters was calculated and reported as the flow. The test was repeated if the discs were not uniformly circular or the major and minor diameters did not match within 1 mm. The mean value from five determinations, expressed to the nearest 1 mm, was recorded as the flow for each experimental group.

2.5.3. Solubility

A mould with an internal diameter of 7 mm and a height of 1 mm was placed on a glass plate and filled with the mixed sealers from each group (n = 10). Another glass plate was pressed on top of the mixed sealers. The mould then was placed in an incubator for 24 h. Subsequently, the samples were removed from the mould, and the discs were weighed three times using an analytical balance with a precision of 0.001 g. The mean mass from the three readings was recorded as the initial mass to the nearest 0.001 g. Each specimen was suspended in a plastic container containing 10 mL of deionised water. The containers were sealed and placed in an incubator for one week. Thereafter, the specimens were removed from their containers and washed with distilled and deionised water. The excess water was removed using absorbent paper. Afterwards, the samples were weighed three times at 15-min intervals to determine the final mass. The material solubility was calculated by the proportion of mass loss identified for each sample and expressed as a percentage of the original mass. The difference between the original and final weight of each sample, determined to the nearest 0.001 g, represented a percentage of the original weight and was used as the solubility of the experimental sealers.

2.5.4. Hardness

The cylindrical specimens (n = 10) with specified dimensions (10 mm in diameter and 2 mm high) were prepared for each experimental group and hand-polished using silicon carbide papers to produce a flat surface. The specimens were stored in 100% relative humidity at 37 °C for one week. The hardness values of specimens were measured using a microhardness tester (V-Test II, Baresiss, Germany) with a Vickers diamond indenter and 100 g load for 20 s. Three Vickers values were recorded for each sample.

2.6. Evaluation of apatite-forming ability of samples

The ability of the added fillers to induce the formation of an apatite-like layer was assessed in an acellular simulated body fluid (SBF) solution.

Disc-shaped specimens (5 mm width and 2 mm height) of each experimental group (n = 3) were immersed in SBF solution at 37 °C and 100% humidity for 3 and 7 days.

The specimens were then removed from the SBF and gently washed and dried at 37°C. The samples before and after immersion in SBF were analyzed using XRD, ATR-FTIR and FESEM-EDX to assess their bioactivity potential and confirm the formation of an apatitic layer. The surface of the specimens was analyzed using an X-ray diffractometer (X'Pert PRO, PANalytical Company, Netherlands) with Cu-Ka radiation of 1.540598 Å at 40 mA, 40 kV, with a scan speed of 0.02 s^{-1}. A spectrometer (ATR-FTIR: ThermoFisher scientific, SMART OMNI-TRANSMISSION, model: NICOLET iS10, USA) was used from 400 to 4000 cm^{-1} with a resolution of 4 cm^{-1} to assess the functional groups in the produced layer. The surface morphology of the specimens was analyzed using FESEM (FEI Nova NanoSEM 450, Netherlands). The elemental composition and mapping of the samples was determined using energy-dispersive X-ray spectroscopy (XFlash 61 10, Bruker AXS Microanalysis, Berlin, Germany) with scanning rate of 2 min.

2.7. Statistical analysis

Before statistical analyses were performed, the normality and homogeneity of the variances of the data were evaluated at a significance level of 5% using the Kolmogorov-Smirnov test and Levene's test, respectively. After confirmation of the normal distribution of the results, two-way analysis of variance (ANOVA) determined the effect of kind and percentage of filler and their interaction on the physical properties of the epoxy-based dental sealers. A post hoc Tukey's HSD for multiple comparisons was used for pairwise comparisons between the study groups. All statistical analyses were executed using SPSS 23.0 for Windows at a significance level of 0.05.

3. Results

3.1. Characterization of synthesized powders

The XRD patterns of the HA, FHA, and BAG samples are shown in (Fig. 1A). The XRD pattern of the BAG sample matched the sodium-calcium-silicate phase ($Na_2Ca_2Si_3O_9$, PDF#0-75-1687) and the main Bragg peaks at ~26°, 32°, 33°, and 34° correspond to the (2 1 1), (3 0 0), (2 0 4), and (2 2 0) Miller planes, respectively. The XRD patterns of HA were consistent with pure HA (JCPDS card #09–0432). The typical peaks of the apatites are at ~26°, 32°, 33°, and 34° and these correspond to the (00 2), (2 1 1), (3 0 0), (2 0 2), and (3 1 0) Miller planes, respectively.

The pattern of FHA was found to be similar to the HA crystalline structure. However, the peaks of (3 0 0) and (2 0 2) at 33° and 34° gradually shifted to higher angles compared to HA and better fit with the FA (JCPDS card #15–0876) XRD pattern (Fig. 1B). All of the diffraction peaks became sharper upon incorporation of fluoride into the HA structure. This indicated an increase in the crystallinity of the FHA crystalline structure (Fig. 1).

In the FTIR spectra, the functional groups of phosphate and carbonate for both HA and FHA were observed (Fig. 2). The presence of carbonate might have originated from the absorption of the carbon dioxide from the atmosphere. The peaks of 472 cm^{-1}, (568 and 607 cm^{-1}), 934 cm^{-1}, 1056 cm^{-1}, are attributed to the ν_2 (P–O), ν_4 (P–O), ν_1 (P–O), and ν_3 (P–O) vibrational bands. Moreover, ν_2 C–O (871 cm^{-1}) and ν_3 C–O (1460–1419 cm^{-1}) vibrational bands were found in both HA and FHA samples. The bands at 1460 and 1419 cm^{-1} and the weak band at 871 $cm^{-1}$are ascribed to the B type carbonate

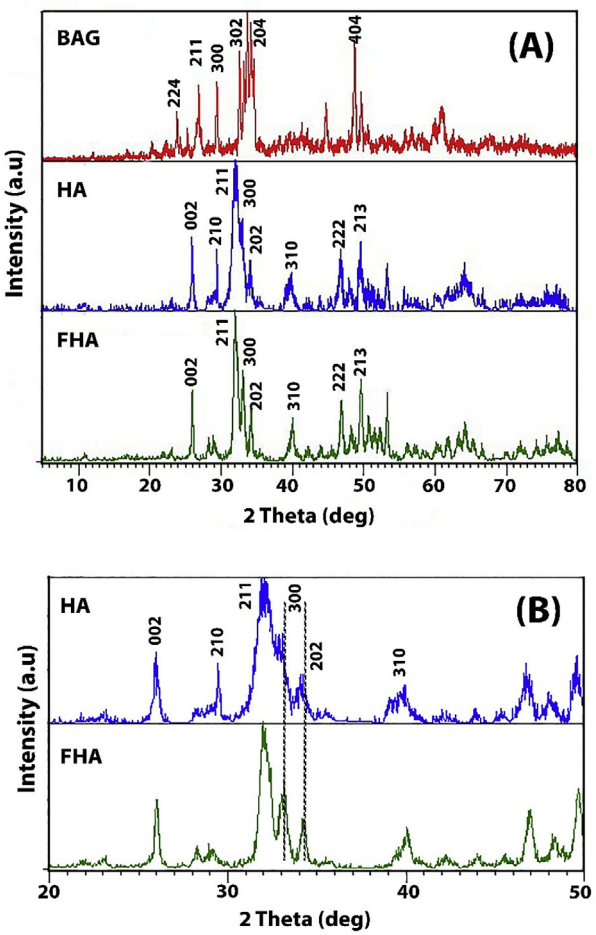

Fig. 1. (A) Broad-range XRD pattern of synthesized powders. (B) Short-range XRD pattern of HA and FHA powders.

resulting from substitution of phosphate ions by carbonate ions [29]. The OH stretching band at 3568 cm^{-1} became weaker with incorporation of fluoride into the HA structure; a new band at 3537 cm^{-1} (OH–F or OH–F–HO) appeared as indicated by the arrow in Fig. 2 [30].

In the FTIR spectra of BAG the bands at 526 and 1046 cm^{-1} can be assigned to the ν_{sym} (Si–O–Si) and ν_{asym} (Si–O–Si) bands of the SiO_4 tetrahedra, respectively. The band at 934 cm^{-1} can be attributed to the SiO_{NBO} (non-bonding oxygen, NBO). A broad peak at 1470 can be attributed to the ν_3 (CO_3^{2-}) band of carbonates adsorbed on the surfaces of synthesized powders [31,32] (Fig. 2).

The microstructure of the powders was examined by FESEM (Fig. 3). A distribution of nano-sized particles with large agglomerates was observed for the BAG and HA powders; these were produced from cold-welding the fine nanoparticles together. The HA powders had a nearly round-shaped morphology and irregular margins with particle sizes ranging 20–40 nm in diameter. The nanometric BAG particles had irregular shapes with particle sizes of 30–60 nm (Fig. 3(a) and (b)).

The microstructure of FHA particles was almost plate-like with different aspect ratios and widths ranged from 200 nm to 1 μm. Layered patterns were seen in the FHA specimens as indicated by the arrows in Fig. 3c.

3.2. Physical properties

Indentations were not visible in all of the specimens after 9 h of storage (the lowest setting available from the manufacturer). The setting time was within the range indicated by the manufacturer, and all of the unmodified and modified specimens passed the ISO 6876 requirements for setting time. The flow value of the experimental sealers ranged from 14.16 to 24.33 mm for the unmodified and FHA/20% samples, respectively. All of the experimental groups, except the FHA-modified samples, had flow values over 20 mm, which agrees well with the ISO 6876 requirements for dental sealers [28]. However, the flow of the modified samples was significantly reduced versus unmodified ones regardless of the filler percentage ($p \leq 0.001$). The difference between the flow values of the FHA-modified groups and both the HA and BG modified groups was also statistically significant ($p \leq 0.001$). However, the flow of HA and BAG-modified sealers was not different ($p = 0.584$).

The solubility data (Table 1) indicates that no specimens underwent more than 1% weight loss, which is under the 3% threshold determined by the ISO standard. The FHA/10% group showed the lowest solubility and even the FHA/20% exhibited a weight gain as the result of water sorption. The difference between the solubility value of the FHA-modified groups and other groups was statistically significant ($p \leq 0.001$). However, the difference between the solubility of the control, HA, and BAG-modified groups was not statistically meaningful ($p > 0.05$).

Table 1 shows that the mean hardness values of the epoxy-based endodontic sealers were significantly increased upon addition of calcium phosphate fillers ($p \leq 0.001$). However, the Vickers microhardness values between the modified groups did not show any statistically significant differences ($p > 0.05$).

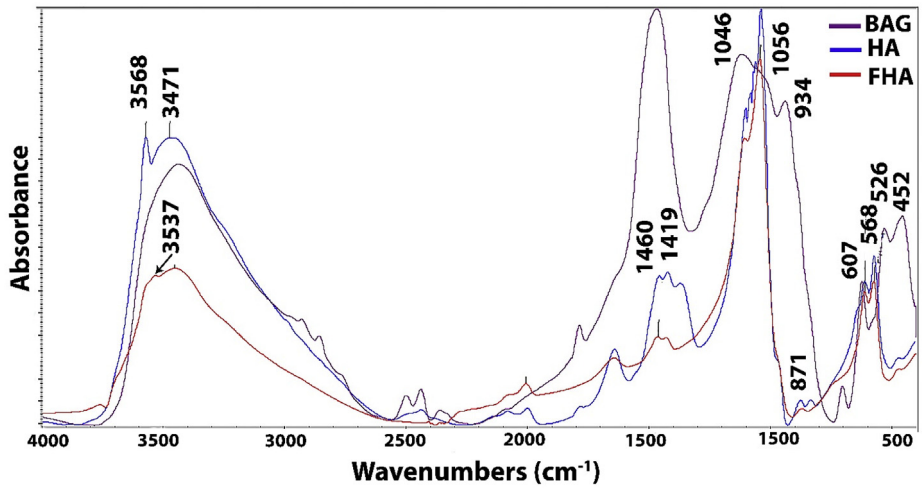

Fig. 2. FTIR spectra of synthesized powders.

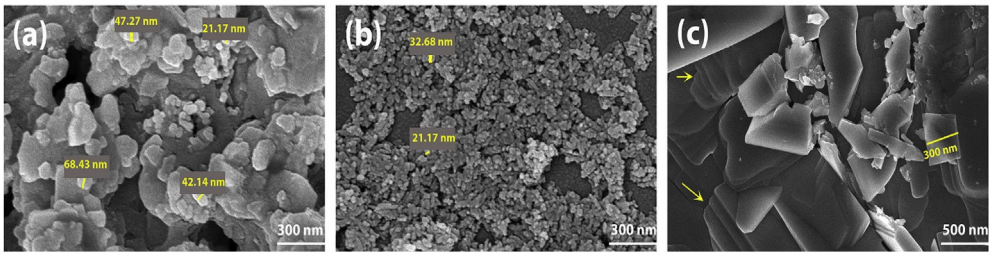

Fig. 3. Field emission scanning electron microscopy micrographs of synthesized (A) bioglass (BAG), (B) hydroxyapatite (HA), and (C) fluorine-substituted hydroxyapatite (FHA).

3.3. Apatite-forming ability of unmodified and modified sealers

The SEM/EDX and EDX mapping images of the specimens before and after 3 and 7 days of soaking in SBF are presented in Figs. 4–7 and Figs. 8–10, respectively. The SEM images show that the nBAG and nHA fillers at both 10 and 20% wt were evenly distributed and dispersed throughout the epoxy resin matrix (Figs. 5A1, 6A1). In contrast, several voids can be seen in the FHA-containing composites probably due to the unequal distribution and agglomeration of the fillers (Fig. 7A1). The SEM images and EDX elemental mapping confirmed the formation of the mineral deposits on the surfaces of all of the modified specimens after 3 and 7 days of immersion in SBF (Figs. 5–7 and Figs. 8–10). The SEM images of the BAG-modified samples showed the creation of a thick and newly developed layer on the surface of the nBAG-containing sealers, which was fractured in different areas due to the drying process (Fig. 5). A similar fractured pattern with lower density was observed in the HA and FHA-modified samples. Calcium phosphate precipitates were also observed in the control group; however, these precipitates were not as well developed as the other groups according to SEM images (Fig. 4). The formation of this thin un-developed calcium-phosphate layer on the surface of unmodified samples maybe resulted from the surface roughness of the samples that may promote the nucleation of calcium-phosphate precipitates [33].

The EDX elemental mapping analysis showed an increase in the Ca and P elements in all modified samples. This confirmed the homogeneous calcium phosphate's deposition (Figs. 8–10). This increase was obvious in BAG and HA-modified samples.

The EDX analysis after 3 days of soaking in SBF revealed that the mineral deposits formed on the surface of all specimens were mainly composed of carbon (C), oxygen (O), bismuth (Bi), calcium (Ca), and phosphorous (P) (Figs. 4–7). The Ca and P content increased in all of the modified and unmodified specimens after immersion in SBF. The highest increase was observed in the BAG-modified groups. There was a remarkable reduction in the Bi in all groups except for the unmodified and FHA/20% groups, which confirmed the formation of a new layer in the BAG, HA, and FHA/10% modified groups.

The ATR-FTIR analysis showed that the absorption bands assigned to the epoxy resin sealer including 1232 cm^{-1} (C–N), 1300 cm^{-1} (C–H), 1505 cm^{-1}(C–H), 1605 cm^{-1}(C–H), 2870 cm^{-1} (C–H), 2920 cm^{-1} (C–H), and 3037 cm^{-1} (C–H) in BAG-modified samples; these peaks decreased or disappeared after 3 or 7 days of immersion in SBF, which suggests the formation of a new layer on the surface of the specimens. The appearance of new absorption bands at 1400 cm^{-1} can be attributed to the formation of carbonated apatite in the BAG and HA-modified sealers (Fig. 11 (B1, B2, C1 and C2)).

A peak at 1031 cm^{-1} in the control group appeared after immersion in SBF solution, which can be attributed to PO_4^{3-}. In the BAG and HA-modified samples, this peak shifted to a lower wave number. The ledge at 1105 cm^{-1} disappeared, and the absorption bands at 1031 cm^{-1} and 1105 cm^{-1} merged to form a new peak at 1108 cm^{-1} and 1027 cm^{-1} in the BAG and HA-modified groups, respectively. The FHA-modified specimens showed a pattern close to the unmodified samples after 3 and 7 days of soaking in SBF particularly in the case of FHA/20% (Fig. 11).

The XRD patterns of the set sealers (Fig. 12) matched with octacalcium phosphate (PDF#0026–1056), HA (PDF#09–0432), and bismuth oxide (PDF#41–1449). The main Bragg peaks were at ~26°, 27°, 28°, 33°, and 35°. It is notable that the peaks of these phases were mostly in the same region.

The control group had a significant increase in the 27° and 28° peaks after immersion in SBF. This increase can be attributed to the formation of immature calcium phosphate precipitates that maybe resulted from the surface roughness of the samples. In the BAG-modified samples, the main Bragg peaks became weaker probably as a result of the formation of a thick new layer. This layer can overshadow the bismuth oxide peaks. Actually, all of the diffracted peaks in the BAG samples can be ascribed to the calcium phosphate components including OCP and HA. In contrast, the XRD pattern of the HA group showed significant increases in the dedicated peaks of apatite at ~26°, 33°, and 35°. No obvious crystallography changes were found in FHA/20% (Fig. 12). It is notable that the XRD was not helpful for evaluation of apatitic layer formation because the aforementioned phases of calcium phosphates and bismuth oxide were mostly in the same region.

4. Discussion

Ideally, root canal sealers should be bioactive, and the bioactivity is related to their composition and constitution. It is important that the added bioactive fillers do not adversely affect the physical properties of the material. Here, we added three different synthesized bioactive submicron sized fillers and evaluated their effect on the physical properties and bioactivity of epoxy-based dental sealers.

The synthesized powders were evaluated using SEM, XRD, and FTIR. The XRD pattern of partially FHA was nearly identical to that of HA, and no structures have been recorded for partially F^-substituted

Table 1
Physical properties of unmodified epoxy sealer and those modified with BAG, HA, and FHA particles (mean ± SD).

	Control	BAG		HA		FHA	
		10%	20%	10%	20%	10%	20%
Flow (mm)	24.33 ± 0.57	21 ± 1^{a}	20.5 ± 0.5^{b}	20.83 ± 0.57^{a}	20.16 ± 0.28^{b}	15.16 ± 0.76	14.16 ± 1.25
Hardness	20.93 ± 1.05	22.36 ± 0.88^{cd}	22.79 ± 1.10^{ef}	22.82 ± 1.73^{c}	22.22 ± 0.53^{e}	23.83 ± 1.39^{d}	23.53 ± 0.68^{f}
Solubility (%reduction in weight)	0.72 ± 0.25^{ghij}	0.65 ± 0.33^{gk}	0.55 ± 0.50^{hl}	0.54 ± 0.39^{ik}	0.72 ± 0.29^{jl}	0.33 ± 0.29	−0.61 ± 0.63

The same letters denote groups that are not statistically significant differences.

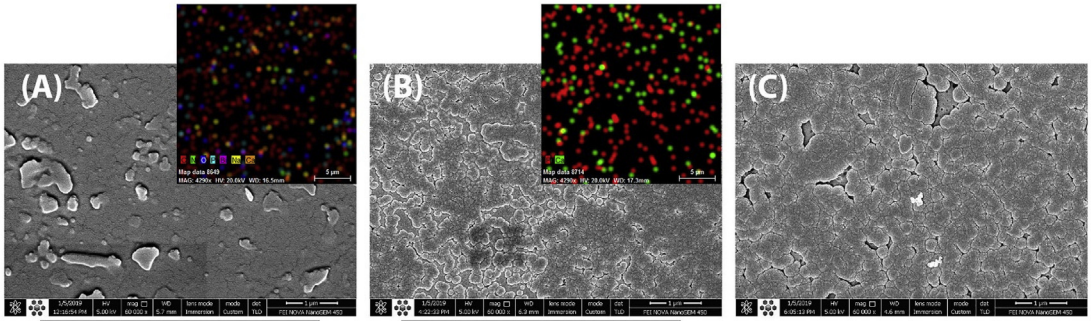

Main compositions	
Element	wt%
C	69.99
O	16.33
Bi	11.10
Ca	0.00
P	0.33

Main compositions	
Element	wt%
C	49.54
O	21.64
Bi	10.83
Ca	5.06
P	5.13

Fig. 4. Representative FESEM images, elemental composition, and EDX elemental mapping of control (unmodified) group. A; before soaking in SBF, B; after 3 days of soaking in SBF, and C; FESEM images of control (unmodified) group after 7 days of soaking in SBF. The Ca and P ions in the figures of EDX elemental mapping are indicated with green and red colours respectively.

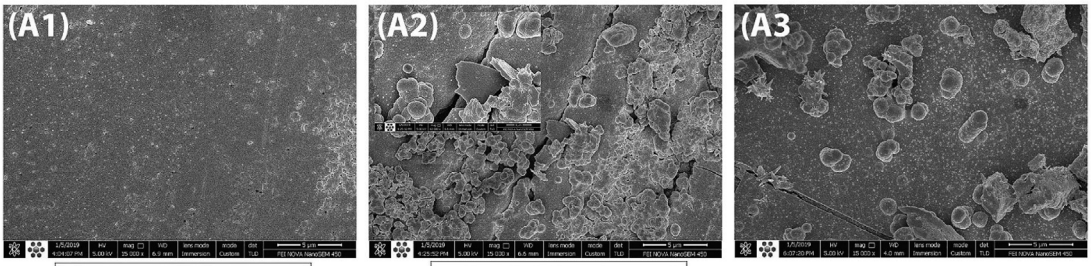

Main compositions	
Element	wt%
C	61.39
O	17.26
Bi	6.22
Ca	4.58
P	1.78

Main compositions	
Element	wt%
C	36.01
O	30.39
Bi	4.27
Ca	18.04
P	7.53

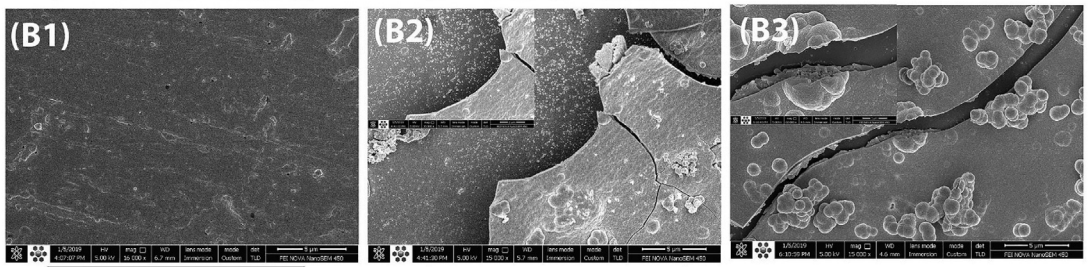

Main compositions	
Element	wt%
C	59.95
O	14.71
Bi	5.52
Ca	4.64
P	2.60

Main compositions	
Element	wt%
C	25.57
O	38.54
Bi	0.21
Ca	16.27
P	10.77

Fig. 5. Representative FESEM images and elemental composition of BAG-modified samples. (A1) 10%-before soaking in SBF; (A2) 10%-after 3 days of soaking in SBF; and (A3) FESEM images of 10% BAG-modified samples after 7 days of soaking in SBF, (B1) 20%-before soaking in SBF, (B2) 20%-after 3 days of soaking in SBF; and (B3) FESEM images of 20% BAG-modified samples after 7 days of soaking in SBF.

apatites in the ICDD database. However, with the incorporation of F^- ion in the HA lattice structure, the peaks of the (3 0 0) and (2 0 2) Miller planes shifted to the right versus the HA pattern (Fig. 1). Incorporation of F^- anions with lower ionic radius decreases the length of *a*-axis of the hexagonal crystal structure and, hence, causes the peaks to shift to higher angles.

The microstructure of the powders was examined by SEM. For the BAG and HA powders, a distribution of nano-sized particles with large agglomerates were observed likely due to cold-welding of the fine nanoparticles together. The HA powders had a nearly round-shaped

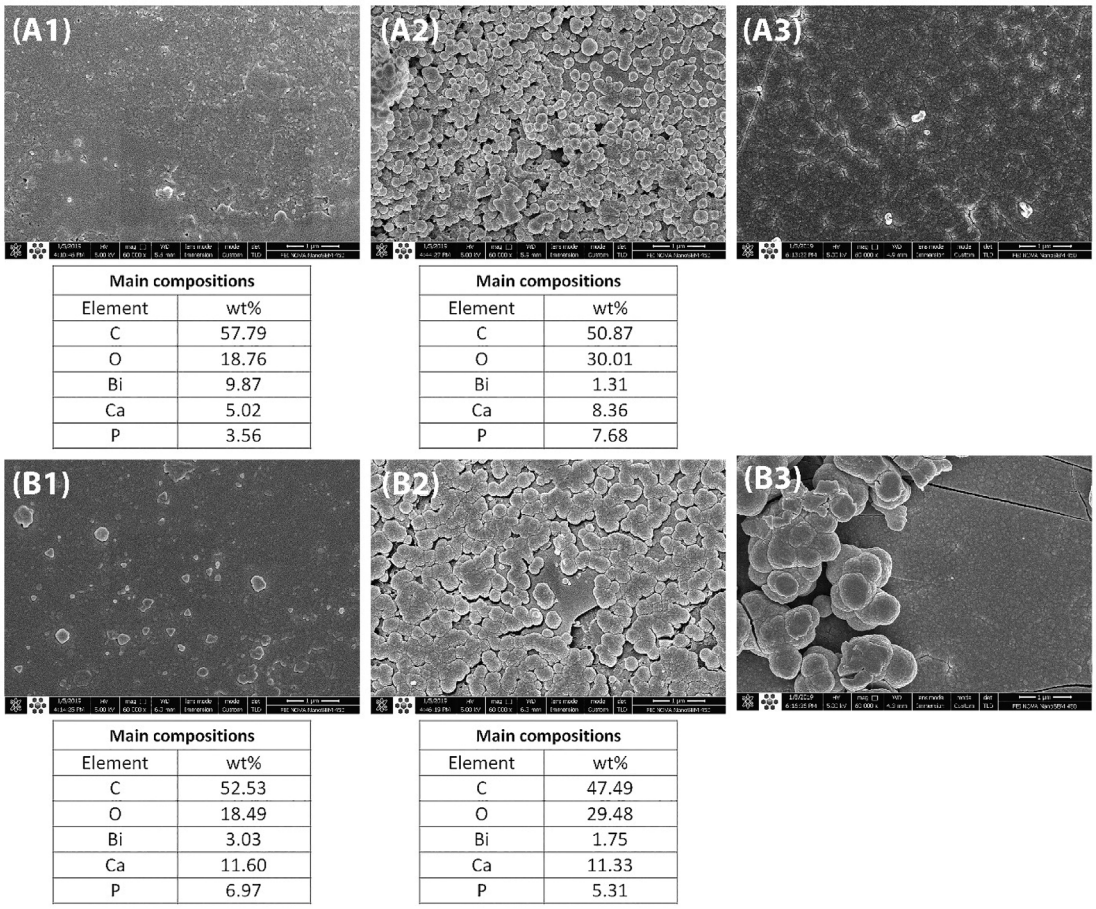

Main compositions	
Element	wt%
C	57.79
O	18.76
Bi	9.87
Ca	5.02
P	3.56

Main compositions	
Element	wt%
C	50.87
O	30.01
Bi	1.31
Ca	8.36
P	7.68

Main compositions	
Element	wt%
C	52.53
O	18.49
Bi	3.03
Ca	11.60
P	6.97

Main compositions	
Element	wt%
C	47.49
O	29.48
Bi	1.75
Ca	11.33
P	5.31

Fig. 6. Representative FESEM images and elemental composition of HA-modified samples. (A1) 10%- before soaking in SBF; (A2) 10%-after 3 days of soaking in SBF; and (A3) FESEM images of 10% HA-modified samples after 7 days of soaking in SBF; (B1) 20%-before soaking in SBF; (B2) 20% after 3 days of soaking in SBF; and (B3) FESEM images of 20% HA-modified samples after 7 days of soaking in SBF.

morphology and irregular margins with particle sizes 20–40 nm in diameter. The nanometric BAG particles had irregular shapes with particle sizes of 30–60 nm.

The microstructure of the FHA particles was almost plate-like with different aspect ratios. Different researchers have determined that the incorporation of F^- ions affects the morphology [25,34] and the mechanical properties of apatite crystals [30]. In this study, fluoride substitution into the apatite crystalline structure altered the morphology of the crystals and increased their aspect ratio. The sharp margins of the FHA crystals were indicative of the highly crystalline nature of crystals (Fig. 2).

Fluoride is known to cause epitaxial growth of crystals on the octacalcium phosphate (OCP) precursor and change the crystal morphology of apatite crystals [35]. Fan et al. [36] reported that fluoride had a dose-dependent effect on the morphology of calcium phosphate crystals [36]. Moreover, other studies suggested that variables like the pH value of reaction solution and temperature can alter the hydroxyapatite morphology and structure [37–39]. In the current study a pH-cycling method was employed to synthesize the FHA powder. The changes in pH during the synthesis procedure can also affect the morphology and size of the particles.

In this study, synthesized powders were added to the endodontic epoxy sealers, and their effect on the physical properties including setting time, flow, solubility, and hardness were examined. The bioactivity of the modified sealers was also evaluated.

A sufficient setting time is important to provide proper consistency for completely filling multi-rooted teeth [40]. According to the ISO 6876, the measured setting time should be within the range claimed by the manufacturer [28]. All evaluated experimental sealers in this study met this criterion. The amount and kind of added fillers did not affect the long-term setting reaction of the epoxy sealers.

High solubility is not desirable in root canal sealing materials because any released materials may irritate the periapical tissues and lead to gaps between the root canal surface and filling materials. These gaps can increase bacterial leakage and lead to failure of the root canal treatment [41]. According to the ISO 6876, the solubility test was based on the original and final weight of the specimens after 24 h of water storage. Standard requirements for root canal sealing materials state that the solubility of a tested material must not be more than 3% of its initial weight. The added fillers did not increase the solubility, and they did not destabilize the highly cross-linked sealer matrix (Table 1). In contrast, the addition of FHA particles into the epoxy sealer significantly reduced its solubility. The addition of 20% FHA increased the weight of the conventional sealer. Different porosities were seen in this group (Figs. 7 A1 and B1), which may lead to a high amount of water sorption and consequently weight increases. The porosities seen here might be produced due to the high viscosity of the FHA-modified samples and non-homogenous distribution of the FHA particles, which mostly were in the micron size range.

A sufficient flow value for an endodontic sealer is an important issue in root canal therapy. It can permit adequate flow to the instrumented canals and avoids flow into the periapical tissues [40]. The rheological properties of a filled polymer composite depend on the contact area between the dispersed (filler) and continuous (polymer) phases and also on the interaction between these phases [42]. The viscosity of the composite are determined by the size of the filler, specific surface area,

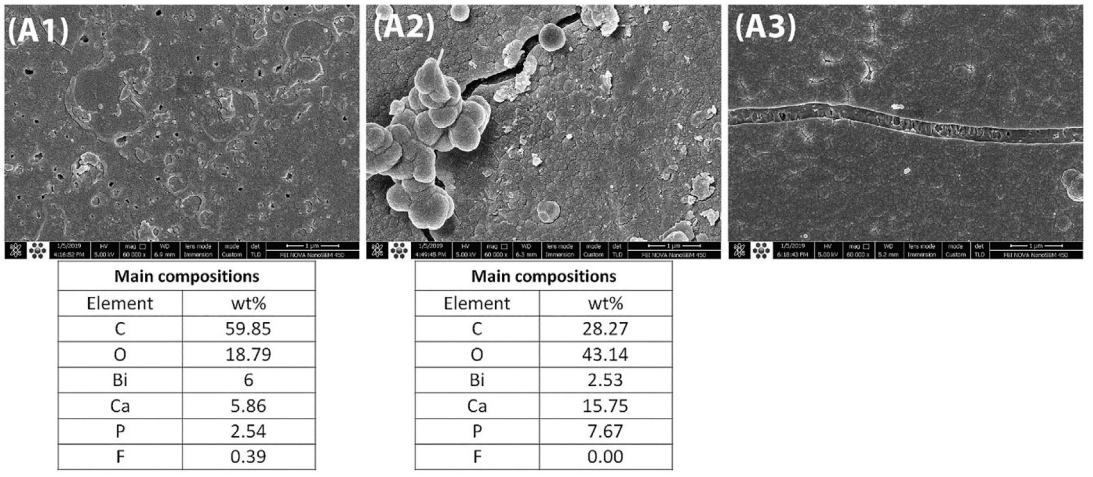

Main compositions	
Element	wt%
C	59.85
O	18.79
Bi	6
Ca	5.86
P	2.54
F	0.39

Main compositions	
Element	wt%
C	28.27
O	43.14
Bi	2.53
Ca	15.75
P	7.67
F	0.00

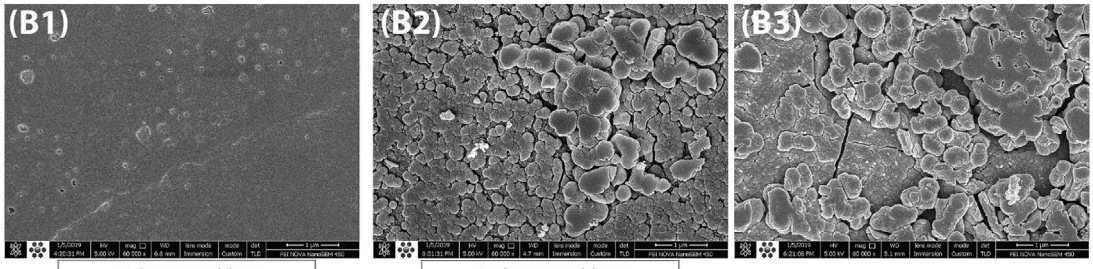

Main compositions	
Element	wt%
C	56.10
O	17.79
Bi	6.33
Ca	7.24
P	5.94
F	0.81

Main compositions	
Element	wt%
C	42.01
O	15.16
Bi	8.44
Ca	5.16
P	4.79
F	0.00

Fig. 7. Representative FESEM images and elemental composition of FHA-modified samples. (A1) 10%-before soaking in SBF; (A2) 10%-after 3 days of soaking in SBF; and (A3) FESEM images of 10% FHA-modified samples after 7 days of soaking in SBF; (B1) 20%-before soaking in SBF, (B2) 20%-after 3 days of soaking in SBF; and (B3) FESEM images of 20% HA-modified samples after 7 days of soaking in SBF.

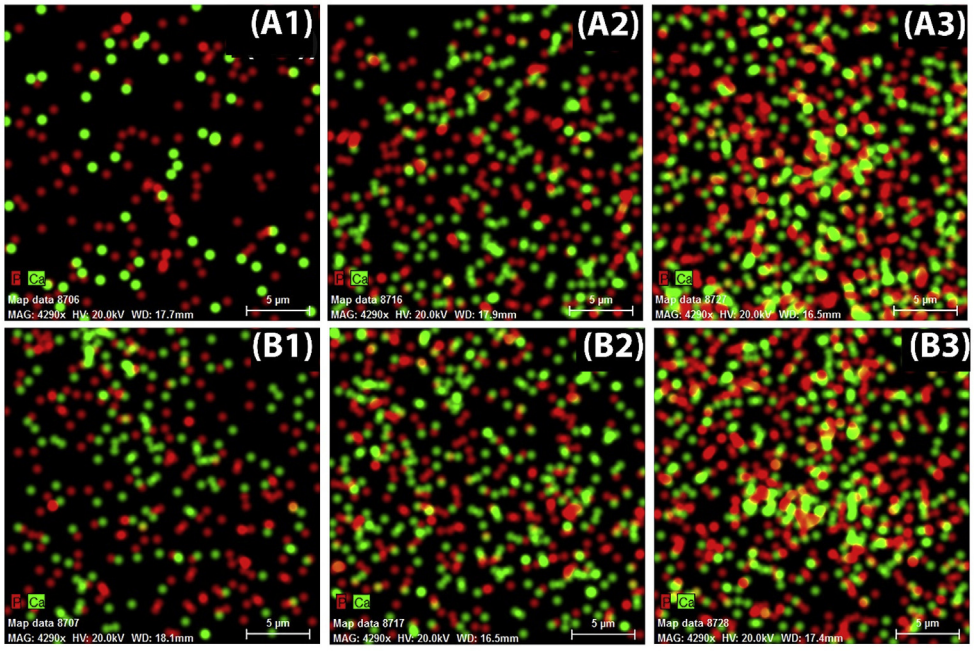

Fig. 8. EDX elemental mapping of BAG-modified samples. (A1) 10%-before soaking in SBF, (A2) 10%-after 3 days of soaking in SBF, (A3) 10%-after 7 days of soaking in SBF, (B1) 20%-before soaking in SBF, (B2) 20%-after 3 days of soaking in SBF, and (B3) 20%-after 7 days of soaking in SBF. The Ca and P ions are indicated with green and red colours respectively.

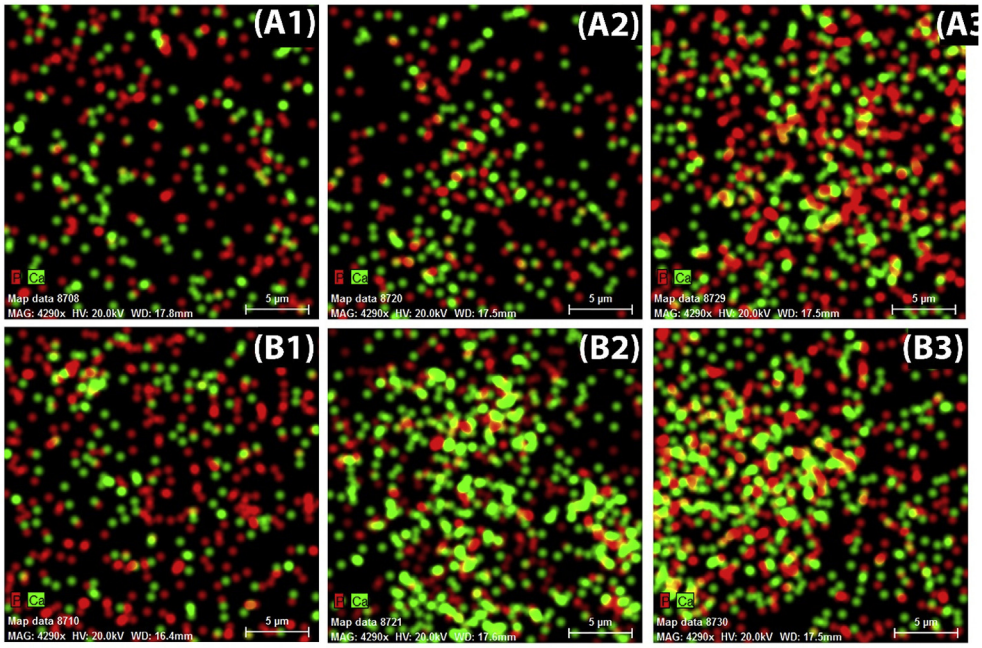

Fig. 9. EDX elemental mapping of HA-modified samples. (A1) 10% before soaking in SBF; (A2) 10% after 3 days of soaking in SBF; (A3) 10% after 7 days of soaking in SBF; (B1) 20%-before soaking in SBF; (B2) 20% after 3 days of soaking in SBF; and (B3) 20% after 7 days of soaking in SBF. The Ca and P ions are indicated with green and red colours respectively.

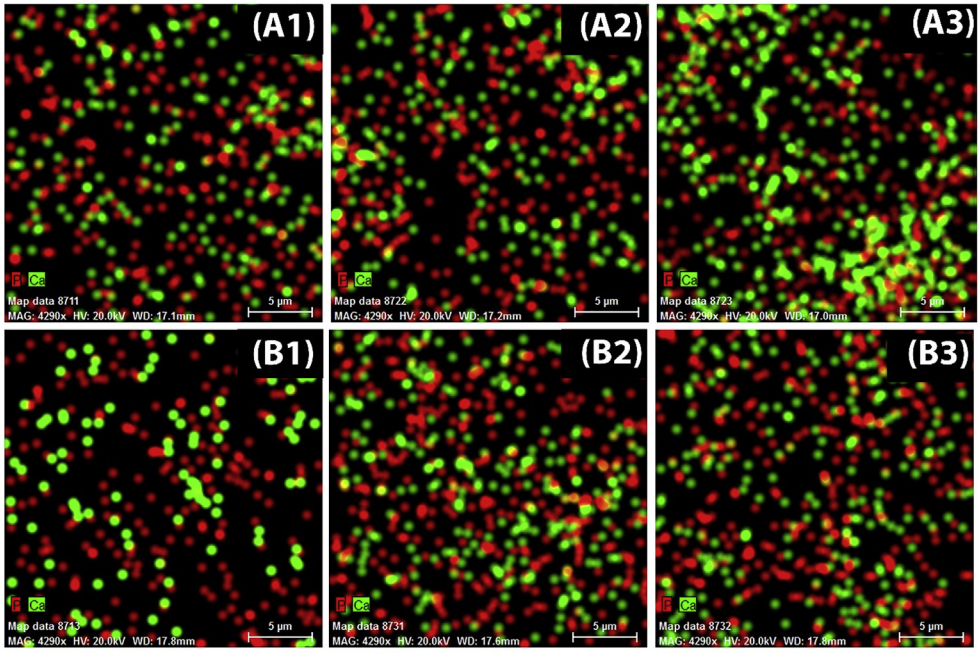

Fig. 10. EDX elemental mapping of FHA-modified samples. (A1) 10%-before soaking in SBF, (A2) 10%-after 3 days of soaking in SBF, (A3) 10%-after 7 days of soaking in SBF, (B1) 20%-before soaking in SBF, (B2) 20%-after 3 days of soaking in SBF, (B3) 20%-after 7 days of soaking in SBF. The Ca and P ions are indicated with green and red colours respectively.

composition, and morphology [42,43], and edges of the fillers [44]. In our study, the FHA fillers significantly reduced the flow of the epoxy resins. High contact area, sharp margins, and the layered form of the plate-like FHA are some factors likely responsible for this sharp reduction in fluidity. The sharp margins may increase the viscosity by harsh frictional contact between the fillers and matrix [44], and the layered plate-like FHA may trap the polymer preventing it from flowing easily and thus increasing its viscosity.

We show here that the hardness values of all modified sealers increased compared to the control group. However, because endodontic sealers should not be exposed to mastication forces, the hardness value of a dental sealer is not an important feature. Nevertheless, the improved surface mechanical properties indicated that the added fillers had a reinforcing effect and did not deteriorate the sealer's structure due to agglomeration or poor dispersion. The agglomeration of the fillers may act as a weak point that leads to the formation of flaws, defects, and the deterioration of the mechanical properties of dental resins [45,46]. The improvements in the hardness values seen here were reflected by the even distribution of the fillers throughout the resin matrix, which did not adversely affect the mechanical properties. Moreover, the fillers likely acted as a crack-deflecting agent that hindered crack propagation through the epoxy matrix. The surface morphology and microstructure of the control and modified groups before and after 3 and 7 days immersing in SBF were characterized using FESEM-EDX, XRD and FTIR. The bioactive materials can initiate calcium phosphate nucleation on their surface from biological fluids [47]. The growth of the Ca–P precipitates on the surfaces of all groups was observed in SEM images after 3 and 7 days of immersion in SBF (Figs. 4–7). The creation of Ca/P depositions was also confirmed by the EDX elemental mapping analysis in representative samples from

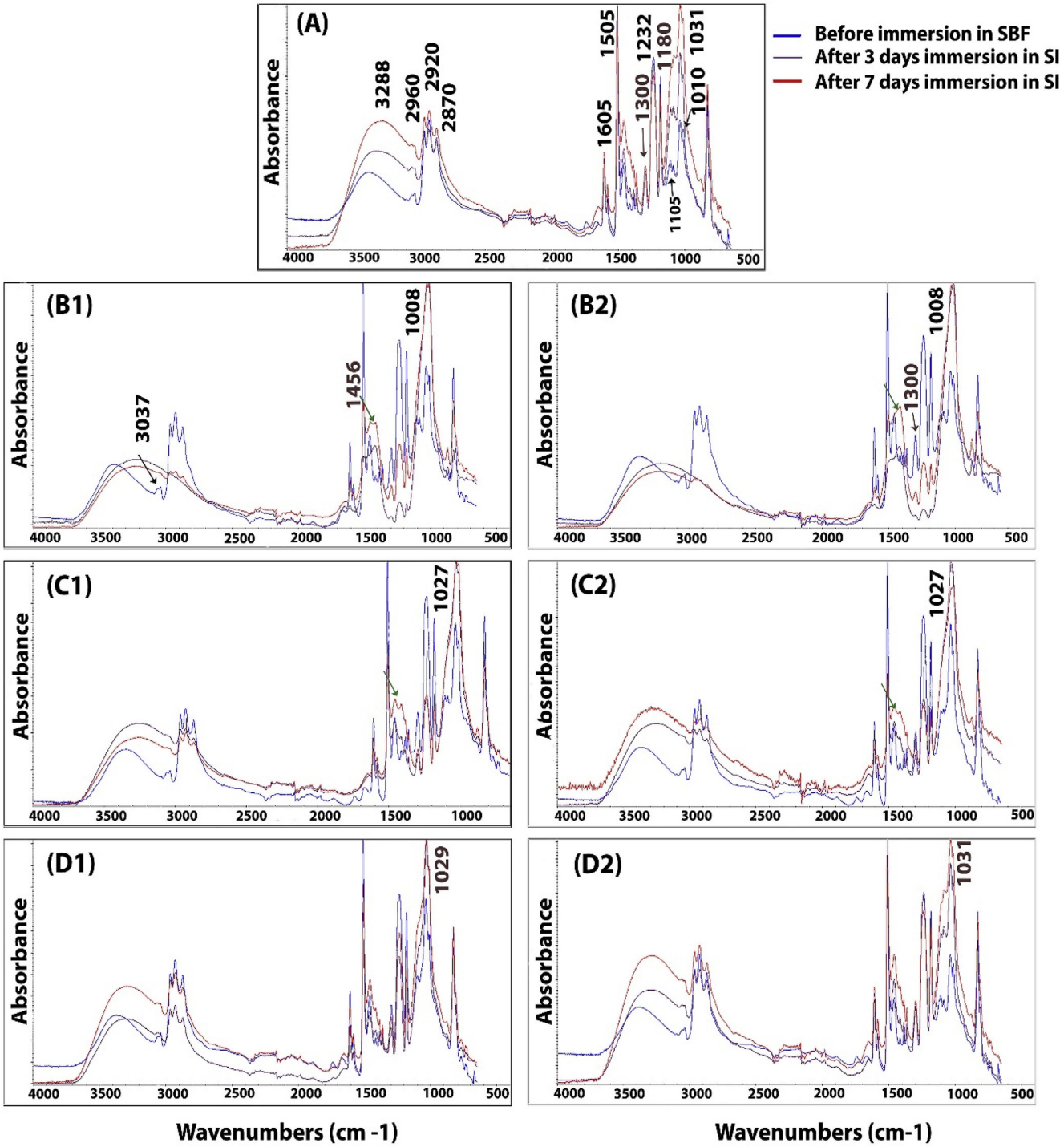

Fig. 11. FTIR spectra of (A) control (unmodified) group; (B1) and (B2) are 10% and 20% BAG-modified groups, respectively; (C1) and (C2) are 10% and 20% HA-modified groups, respectively; and (D1) and (D2) are 10% and 20% FHA-modified groups, respectively.

modified groups (Figs. 8–10).

A thick new layer was created in the BAG-containing sealers (Fig. 5). The ATR-FTIR showed that, for the BAG-containing samples, the bands at ~2870 cm^{-1}, ~2920 cm^{-1}, ~2960 cm^{-1} and ~3288 cm^{-1} were ascribed to the (C–H) groups related to the epoxy composition, disappeared after soaking in SBF. Moreover, the intensity of the other band assigned to the epoxy sealer, including the bands at ~825 cm^{-1} (C–H), ~1230 cm^{-1} (C–N) stretch mode, and ~1300 cm^{-1} (C–H) significantly decreased (Fig. 11 (B)). After soaking in SBF, the presence of $PO4^{3-}$ stretch mode was observed in the control group at 1,031 cm^{-1}, which shifted to a higher wavenumber in the BAG and HA-modified samples (Fig. 11 (B) an (C)). It has been reported that the bands corresponding to the PO_4^{3-} group at ~1030 cm^{-1} can be attributed to OCP, and around 1003 cm^{-1} can be attributed to HA [48].

Accordingly, the layer created in the BAG-modified samples is likely a hydroxyapatite layer and the Ca/P precipitation on the surface of the control group is mostly OCP. The formation of this un-developed calcium phosphate layer maybe resulted from the surface roughness of unmodified specimens. The appearance of new absorption bands in the BAG and HA-containing sealers at ~1400 cm^{-1} can be assigned to C–O

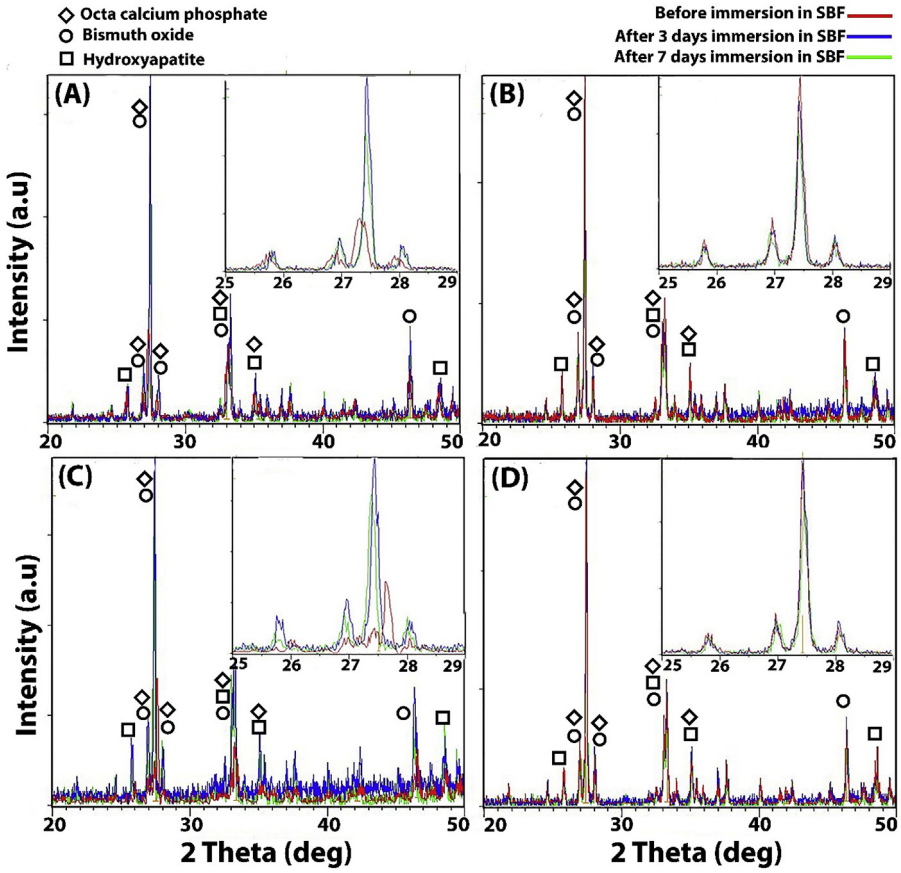

Fig. 12. XRD pattern of (A) Control (unmodified) group, (B) 20% BAG-modified group, (C) 20% HA-modified group, and (D) 20% FHA-modified group.

stretching vibration and therefore, to the formation of carbonated apatite that mimics the apatite of bone and dental hard tissues.

The materials can be categorized into “active” and “passive” biomaterials according to the process of apatite formation on the surface. Active biomaterials release ions via diffusion, dissolution, and hydrolysis into biological fluids. This increases the supersaturation, which results in the fast formation of an apatitic layer [47]. Researchers have determined that the BAG are active biomaterials that release ions via diffusion into the biological fluids (47). In the present study, we did not measure the released ions into the SBF. However, according to the literature (47) the formation of a dense mineral compound on the BAG-modified samples may be attributed to the $PO4^{3-}$and the Ca^{2+} ions diffusion into the SBF solution. Apatites act as passive biomaterials that prepare an appropriate substrate for heterogeneous nucleation [47]. In the HA-containing samples, the HA particles led to a negative surface charge that can bind to positively charged Ca^{2+} ions from the SBF solution; thus, calcium-rich HA formed. Subsequently, the positively charged surface, resulting from Ca^{2+} accumulation, bound to the negatively charged PO_4^{3-} ions and formed a metastable amorphous calcium phosphate layer that ultimately transformed into a stable bone-like apatite [49,50]. Some studies determined that the apatitic layer formation on the surface of composites reinforced with HA fillers in the SBF solution may resulted from the dissolution of HA particles which can lead to the supersaturation of Ca^{2+} and PO_4^{3-} and promote the nucleation and growth of HA crystals [51].

FHA was expected to have the same results as HA due to the negative surface charge [52]. However, there was no obvious apatite layer formation compared to the control group after 7 days in SBF—this is likely due to the different morphologies, particle sizes, or agglomeration of particles. It has to be considered that the synthesis procedure of FHA powder employed in this study was different from HA, that led to the larger size of particles. For better comparison of apatite-forming ability of the particles, future studies have to carefully control the sizes of fillers via the same condition of synthesis procedure. On the other hand, the FHA-modified samples may need more time to show apatite-forming ability.

It is worth considering that, in the case of the BAG-modified sealers, a thick carbonated apatite layer as seen in ATR- FTIR and FESEM-EDX has not been shown using XRD. This probably was due to the overlapping of main Bragg peaks of apatite and bismuth oxide or fracture of the thick produced apatitic layer during XRD analysis procedure. The XRD patterns of the set sealers are shown in Fig. 12. These matched with the OCP (PDF#0026–1056), hydroxyapatite (PDF#09–0432), and bismuth oxide (the main composition of epoxy sealer) (PDF#41–1449). The main Bragg peaks were at ~26°, 27°, 28°, 33°, and 35°. The peaks in these phases were mostly in the same region, and thus the XRD was not helpful for revealing calcium phosphate peaks.

5. Conclusion

Based on the results of this study, it can be concluded that the physical properties of epoxy-based dental sealers are not altered by the addition of BAG and HA nanoparticles up to 20%. The BAG and HA nanofillers enhanced the *in vitro* apatite-forming ability of the epoxy resin sealer. In particular, the formation of a crystalline apatite layer was accelerated in the case of the BAG-modified samples after a short period of soaking in SBF. On the other hand, the incorporation of 20% FHA particles reduced the flow of the epoxy sealer and did not improve the apatitic layer formation compared to the unmodified samples. Thus, according to the results of this preliminary study, the incorporation of nano-structured BAG and HA fillers represents a promising approach for the reinforcement of resin-based endodontic sealers.

It is notable that in our study the size and morphology of prepared FHA particles was different than the HA particles probably due to the

fluoride incorporation or synthesis procedures. Future studies should carefully control these sizes for better comparison. The antibacterial properties of the added fillers should also be considered in future studies.

Acknowledgements

This research has been supported by International Campus of Tehran University of Medical Sciences (IC-TUMS) and health Services grant No. 9423684001.

Appendix A. Supplementary data

Supplementary data to this article can be found online at https://doi.org/10.1016/j.bioactmat.2019.10.004.

References

[1] D. Khandelwal, N.V. Ballal, Recent advances in root canal sealers, Int. J. Clin. Dent. 9 (2016) 3.
[2] R. Johns, Endodontics–science and practice: a textbook for student and practitioner, J. R. Soc. Med. 75 (1982) 574.
[3] P. Neelakantan, S. Sharma, H. Shemesh, P.R. Wesselink, Influence of irrigation sequence on the adhesion of root canal sealers to dentin: a Fourier transform infrared spectroscopy and push-out bond strength analysis, J. Endod. 41 (2015) 1108–1111.
[4] M.R. Leonardo, L. Da Silva, W. Almeida, L.S. Utrilla, Tissue response to an epoxy resin-based root canal sealer, Dent. Traumatol. 15 (1999) 28–32.
[5] R. Viapiana, J.M. Guerreiro-Tanomaru, M.A. Hungaro-Duarte, M. Tanomaru-Filho, J. Camilleri, Chemical characterization and bioactivity of epoxy resin and Portland cement-based sealers with niobium and zirconium oxide radiopacifiers, Dent. Mater. 30 (2014) 1005–1020.
[6] F. Collares, V. Leitune, F. Rostirolla, R. Trommer, C. Bergmann, S. Samuel, Nanostructured hydroxyapatite as filler for methacrylate-based root canal sealers, Int. Endod. J. 45 (2012) 63–67.
[7] H.O. Simila, N. Karpukhina, R.G. Hill, Bioactivity and fluoride release of strontium and fluoride modified Biodentine, Dent. Mater. 34 (2018) e1–e7.
[8] R.A. Alhashimi, F. Mannocci, S. Sauro, Bioactivity, cytocompatibility and thermal properties of experimental Bioglass-reinforced composites as potential root-canal filling materials, J. Mech. Behav. Biomed. Mater. 69 (2017) 355–361.
[9] S. Heid, P.R. Stoessel, T.T. Tauböck, W.J. Stark, M. Zehnder, D. Mohn, Incorporation of particulate bioactive glasses into a dental root canal sealer, Biomed. Glasses 2 (2016).
[10] C. Corral Nunez, C. Covarrubias, E. Fernandez, OBd Oliveria Junior, Enhanced bioactive properties of BiodentineTM modified with bioactive glass nanoparticles, J. Appl. Oral Sci. 25 (2017) 77–185.
[11] A. Kishen, Nanotechnology in Endodontics, Springer, 2016.
[12] Z. Tarle, Bioaktivni dentalni kompozitni materijali, Rad. Hrvat. Akad. Znan. i Umjet. Med. Znan. 533 (2018) 83–99.
[13] S.V. Dorozhkin, M. Epple, Biological and medical significance of calcium phosphates, Angew. Chem. Int. Ed. 41 (2002) 3130–3146.
[14] S. Mahalakshmi, K. Selvaraju, Growth and characterization of hexamine single crystal, Int. J. Chem. Sci. 11 (2013) 1831–1837.
[15] R. Wang, S. Bao, F. Liu, X. Jiang, M. Zhu, Design of resin composites with enhanced physical–mechanical properties, Mater. Res. Innov. 18 (2014) S4–S812 S4-816.
[16] T.O. Mon Mon, V. Gopalakrishnan, A. Samsuddin, K. Al Salihi, O. Shamsuria, Antibacterial property of locally produced hydroxyapatite, Arch. Orofac. Sci. 2 (2007) 41–44.
[17] P. Makvandi, C. Esposito Corcione, F. Paladini, A.L. Gallo, F. Montagna, R. Jamaledin, M. Pollini, A. Maffezzoli, Antimicrobial modified hydroxyapatite composite dental bite by stereolithography, Polym. Adv. Technol. 29 (2018) 364–371.
[18] C. Santos, Z. Luklinska, R. Clarke, K. Davy, Hydroxyapatite as a filler for dental composite materials: mechanical properties and *in vitro* bioactivity of composites, J. Mater. Sci. Mater. Med. 12 (2001) 565–573.
[19] M. Mathew, S. Takagi, Structures of biological minerals in dental research, J. Res. Natl. Inst. Stand. Technol. 106 (2001) 1035.
[20] L. Rintoul, E. Wentrup-Byrne, S. Suzuki, L. Grøndahl, FT-IR spectroscopy of fluoro-substituted hydroxyapatite: strengths and limitations, J. Mater. Sci. Mater. Med. 18 (2007) 1701–1709.
[21] M. Wei, J. Evans, T. Bostrom, L. Grøndahl, Synthesis and characterization of hydroxyapatite, fluoride-substituted hydroxyapatite and fluorapatite, J. Mater. Sci. Mater. Med. 14 (2003) 311–320.
[22] T. Aoba, The effect of fluoride on apatite structure and growth, Crit. Rev. Oral Biol. Med. 8 (1997) 136–153.
[23] E.C. Moreno, M. Kresak, R.T. Zahradnik, Fluoridated hydroxyapatite solubility and caries formation, Nature 247 (1974) 64.
[24] E. Eanes, Enamel apatite: chemistry, structure and properties, J. Dent. Res. 58 (1979) 829–836.
[25] F. Shafiei, M. Behroozibakhsh, F. Moztarzadeh, M. Haghbin-Nazarpak, M. Tahriri, Nanocrystalline fluorine-substituted hydroxyapatite [Ca 5 (PO 4) 3 (OH) 1-x F x (0≤ x≤ 1)] for biomedical applications: preparation and characterisation, IET Micro Nano Lett. 7 (2012) 109–114.
[26] M.S. Bahniuk, H. Pirayesh, H.D. Singh, J.A. Nychka, L.D. Unsworth, Bioactive glass 45S5 powders: effect of synthesis route and resultant surface chemistry and crystallinity on protein adsorption from human plasma, Biointerphases 7 (2012) 41 7.
[27] G. Schmalz, D. Arenholt-Bindslev, Biocompatibility of Dental Materials vol. 1, Springer, 2009.
[28] I. International Organization for Standardization, Dentistry — Root Canal Sealing Materials, (2012).
[29] F. Bollino, E. Armenia, E. Tranquillo, Zirconia/hydroxyapatite composites synthesized via Sol-Gel: influence of hydroxyapatite content and heating on their biological properties, Materials 10 (2017) 757.
[30] W. Qiao, Q. Liu, Z. Li, H. Zhang, Z. Chen, Changes in physicochemical and biological properties of porcine bone derived hydroxyapatite induced by the incorporation of fluoride, Sci. Technol. Adv. Mater. 18 (2017) 110–121.
[31] M. Mačković, A. Hoppe, R. Detsch, D. Mohn, W.J. Stark, E. Spiecker, A. Boccaccini, Bioactive glass (type 45S5) nanoparticles: *in vitro* reactivity on nanoscale and biocompatibility, J. Nanoparticle Res. 14 (2012) 966.
[32] B.C. Bunker, D.R. Tallant, T. Headley, G.L. Turner, R. Kirkpatrick, The structure of leached sodium borosilicate glass, Phys. Chem. Glasses 29 (1988) 106–120.
[33] M. Pisarek, A. Roguska, L. Marcon, M. Andrzejczuk, Biomimetic and electrodeposited calcium-phosphates coatings on Ti–formation, surface characterization, biological response, Biomed. Eng. Tech. Appl. Med. (2012) 3–46.
[34] E. Eanes, A. Hailer, The effect of fluoride on the size and morphology of apatite crystals grown from physiologic solutions, Calcif. Tissue Int. 63 (1998) 250–257.
[35] M. Iijima, H. Tohda, H. Suzuki, T. Yanagisawa, Y. Moriwaki, Effects of F-on apatite-octacalcium phosphate intergrowth and crystal morphology in a model system of tooth enamel formation, Calcif. Tissue Int. 50 (1992) 357–361.
[36] Y. Fan, Z. Sun, J. Moradian-Oldak, Effect of fluoride on the morphology of calcium phosphate crystals grown on acid-etched human enamel, Caries Res. 43 (2009) 132–136.
[37] M. Sadat-Shojai, M.-T. Khorasani, E. Dinpanah-Khoshdargi, A. Jamshidi, Ynthesis methods for nanosized hydroxyapatite with diverse structures, Acta Biomater. 9 (2013) 7591–7621.
[38] J. Liu, X. Ye, H. Wang, M. Zhu, B. Wang, H. Yan, The influence of pH and temperature on the morphology of hydroxyapatite synthesized by hydrothermal method, Ceram. Int. 29 (2003) 629–633.
[39] M. Manoj, R. Subbiah, D. Mangalaraj, N. Ponpandian, C. Viswanathan, K. Park, Influence of growth parameters on the formation of hydroxyapatite (HAp) nanostructures and their cell viability studies, Nanobiomedicine 2 (2015) 2.
[40] D. Ørstavik, Physical properties of root canal sealers: measurement of flow, working time, and compressive strength, Int. Endod. J. 16 (1983) 99–107.
[41] M.K. Wu, P. Wesselink, J.A. Boersma, 1-year follow-up study on leakage of four root canal sealers at different thicknesses, Int. Endod. J. 28 (1995) 185–189.
[42] E. Kuzdzal, B. Cichy, S. Dulik, Morphological properties of fillers for polymeric materials; the influence on rheological properties of compositions with unsaturated polyester resin, Chemik 70 (2016) 189–192.
[43] J.H. Lee, C.M. Um, I.B. Lee, Rheological properties of resin composites according to variations in monomer and filler composition, Dent. Mater. 22 (2006) 515–526.
[44] A.V. Shenoy, Rheology of Filled Polymer Systems, Springer Science & Business Media, 2013.
[45] E. Korkut, E. Torlak, M. Altunsoy, Antimicrobial and mechanical properties of dental resin composite containing bioactive glass, J. Appl. Biomater. Funct. Mater. 14 (2016) e296–e301.
[46] M. Sadat-Shojai, M. Atai, A. Nodehi, L.N. Khanlar, Hydroxyapatite nanorods as novel fillers for improving the properties of dental adhesives: synthesis and application, Dent. Mater. 26 (2010) 471–482.
[47] P. Ducheyne, Comprehensive Biomaterials II, Elsevier, 2017.
[48] W. Mróz, A. Bombalska, B. Budner, S. Burdyńska, M. Jedyński, A. Prokopiuk, E. Menaszek, A. Ścisłowska-Czarnecka, A. Niedzielska, K. Niedzielski, Comparative study of hydroxyapatite and octacalcium phosphate coatings deposited on metallic implants by PLD method, Appl. Phys. A 101 (2010) 713–716.
[49] T. Kokubo, T. Himeno, H.M. Kim, K. Masakazu, T. Nakamura, In Process of bonelike apatite formation on sintered hydroxyapatite in serum-containing SBF, Key Eng. Mater. (2004) 139–142. Trans Tech Publ.
[50] T. Himeno, H.M. Kim, H. Kaneko, K. Masakazu, T. Kokubo, T. Nakamura, In Surface structural changes of sintered hydroxyapatite in terms of surface charge, Key Eng. Mater. (2003) 457–460. Trans Tech Publ.
[51] X.Y. Lin, H.S. Fan, X.D. Li, M. Tang, X.D. Zhang, Evaluation of bioactivity and cytocompatibility of nano-hydroxyapatite/collagen composite in vitro, Key Eng. Mater. (2005) 553–556. Trans Tech Publ.
[52] M.S. Tung, D. Skrtic, Interfacial properties of hydroxyapatite, fluoroapatite and octacalcium phosphate, Monogr. Oral Sci. 18 (2001) 12–29.